8

A HIGH-FREQUENCY NOISE MEASUREMENT SETUP FOR MCBJ

Manohar KUMAR, Mohammed SAGHIR, Stefan STAHL, Bert CRAMA, Ruud VAN EGMOND, Jan VAN RUITENBEEK

We report on the realization of a fast and sensitive broadband high frequency (300kHz – 10MHz) noise measurement setup for the study of fluctuations in the non-equilibrium electric current in mechanically controllable break junctions at cryogenic temperatures. The setup relies on a combination of a cryogenic amplifier plus a room-temperature amplifier stage with a custom built FPGA cross correlator. We have incorporated a two-channel noise detection scheme allowing us to measure the cross spectrum, giving a noise power sensitivity an order of magnitude below the amplifier noise floor. We describe the principle of the set up, its implementation and its calibration. This system is ideal for high-bias noise measurements for the investigation of electron scattering on non-equilibrium vibrons in metal-molecule-metal junctions.

8.1 MOTIVATION AND CONCEPT

THE shot noise measurements on Au atomic contacts above the vibron energy show a linear deviation from the Lesovik-Levitov behavior [1]. The fact that the observed deviation is linear is believed to be due to a strong coupling of the vibrons to the phonon bath in the metallic leads. For weak vibron-phonon relaxation the life time of the vibron becomes long enough for the electrons to see a highly non-equilibrium occupation of vibrons, which would lead to non-linear deviations from the Lesovik-Levitov behaviour. Only in a few cases we have observed a quadratic deviation from the classical Lesovik-Levitov expression (section 4.5), but the degree of vibron coupling to the phonon bath cannot be easily controlled for this system. In the Au atomic chains the vibrons typically decay faster that the average electron-vibron scattering time.

Ideal candidates for the investigation of non-equilibrium vibrons would be the simple molecular junction systems Pt-D_2-Pt[2], or Au-O_2-Au[3]. The vibron energies for these molecular systems lie well above the Debye energy of the metal atoms in the leads, which is important for a small relaxation rate. The lowest vibron energy of the D_2 molecule in Pt-D_2-Pt junction is 38 ± 5meV and for O_2 in Au-O_2-Au it is 49 ± 6mV. For observation of the non-equilibrium noise properties we need to measure at bias voltages eV well above these energies. However, in these molecular contacts the noise spectra show stronger $1/f$ noise as compared to pure Au atomic contacts, and the $1/f$ noise grows even stronger at higher bias. Shot noise is proportional to the bias voltage while $1/f$ noise is proportional to the square of the bias voltage. This leads to a dominance of $1/f$ noise over the shot noise at high bias for the noise measurements in the frequency window that we have used for the experiments described in chapters 4–7 [4, 5]. An example of a spectrum for Au-O_2-Au dominated by $1/f$ noise is shown in figure (1.8b). The linear extrapolation of the $1/f$ noise crosses the white shot noise level at a frequency that we will call the corner frequency of $1/f$ noise. For bias values up to 50mV the $1/f$ corner frequency for Au-O_2-Au is in the order of 400kHz - 500kHz. The measurement bandwidth for the set up described in the previous chapters is limited by the high intrinsic capacitance of the coax running from the sample at cryogenic temperatures to the amplifier at room temperature (RT). This gives a roll off of 30kHz - 40kHz for a sample conductance of $1G_0$. In order to be able to measure the spectrum above the $1/f$ noise corner frequency we need to increase the frequency range of our measurement set up. For the measurements of inelastic scattering above the vibron energies in the molecular systems mentioned above we need to expand the frequency range into the MHz regime.

In order to measure the noise at higher bias one needs to increase the cut off frequency. One of way of increasing the high end frequency cut off is to reduce

the effective impedance of the measurement circuit seen at the input of the noise amplifier. This can be done by using an impedance transformer or an LC tank circuit, but this narrows the bandwidth. Since we have seen many times that it is of great value to be able to verify the white character of the noise, we prefer to maintain a broad band noise measurement. Another solution would be to use a potential divider [6]. Although this helps to maintain a wide band and will shift the cutoff frequency, it also reduces the effective signal feeding into the amplifier. In stead of modifying the effective impedance of the sample we decided to reduce the effective capacitance of the cables running from the sample to the first stage amplifier. This is done by installing the first stage amplifiers as close as possible to the sample so that the wires can be kept short. For this purpose we use low noise cryogenic amplifiers, as has been demonstrated in refs. [7, 8]. The amplifier close to sample reduces the input capacitance of the circuit, while the output impedance of the cryogenic amplifier is matched to the 75Ω transmission line and the input impedance of the RT amplifier. This technique allow us to measure into the MHz regime, up to $f_h \sim 5$MHz. The addition of a $1:2$ potential divider at the input of the first amplifier could increase the measurement bandwidth to 10MHz.

The implementation of the high frequency measurement setup for mechanically controllable break junctions imposes a few design constraints. It requires three parallel engineering routes to custom develop the complete high frequency measurement setup. These three routes shown in figure (8.1) are: (a) The dipstick (b) The two channel spectrum analyzer (c) The low temperature amplifier, which will be described each in a separate section below.

8.2 THE MCBJ DIPSTICK

THE design of the dipstick was based upon an earlier design for a MCBJ dipstick. The new design is made with the purpose of fighting the parasitic capacitance of the wires coupling the sample to the input of the amplifier. This requires placing two cryogenic amplifiers within a few mm distance (~ 5mm) from the sample, that should operate at the bath temperature of 4.2K. The working temperature of the amplifier affects its gain and noise performance drastically so it requires good thermalization of the all the wires going to and out from the cryogenic amplifier. Hence, in the design special attention is paid to cooling and temperature stabilization of the cryogenic amplifiers. In the new design the cryo block at sample end is made as local ground, but we keep the piezo electric control circuit ground separated from sensitive ground. We have used a low-voltage type piezo element with positive bias polarity. The ceramic insulated piezo actuator has dimensions $3\times3\times9$mm with nominal working displacement of 6.5μm ±20% for the full voltage range (0 – 100V) at room temperature.

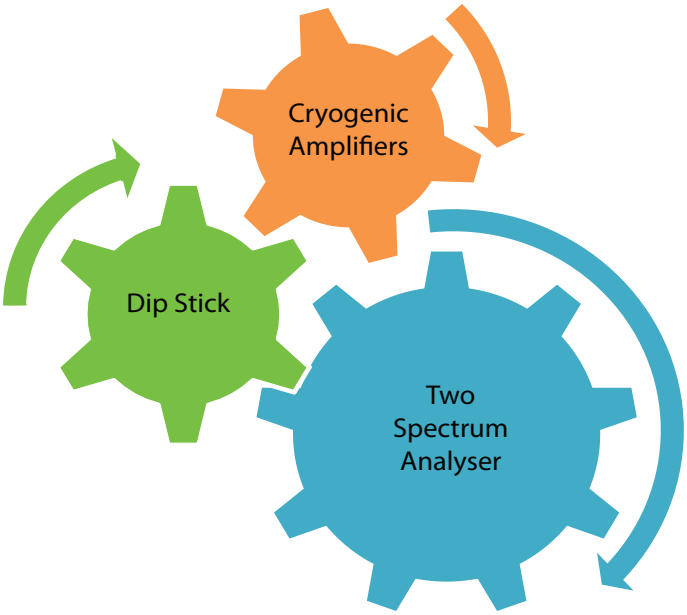

FIGURE 8.1: Churn of technology: Three distinct developments needed for a high frequency noise measurement setup compatible with the MCBJ technique - (a) The dipstick (b) The cryogenic amplifier (c) The two channel spectrum analyzer.

8.2.1 DIPSTICK DESIGN

An image of the bottom part of the dipstick is shown in figure (8.2). We will discuss each of the main design principles in the following paragraphs. In some cases we needed to find compromises in design and working principle. Further improvements in the design will be discussed at the end of this chapter. A detailed schematic of the cryo head and of the RT head of the dipstick are shown in figures (8.3) and (8.4).

Modular design

We paid special attention to make our design modular. The main modular components of our dipstick are: (i) Head (ii) Slot for the cryogenic amplifiers (iii) Cryogenic cap (iv) Wiring capsules. These four parts are coupled together and can be changed without affecting the other parts, within some design constraints. This provides a geat advantage when changes in the cryo-electronics, cryo-head or the wiring scheme are required for future new developments.

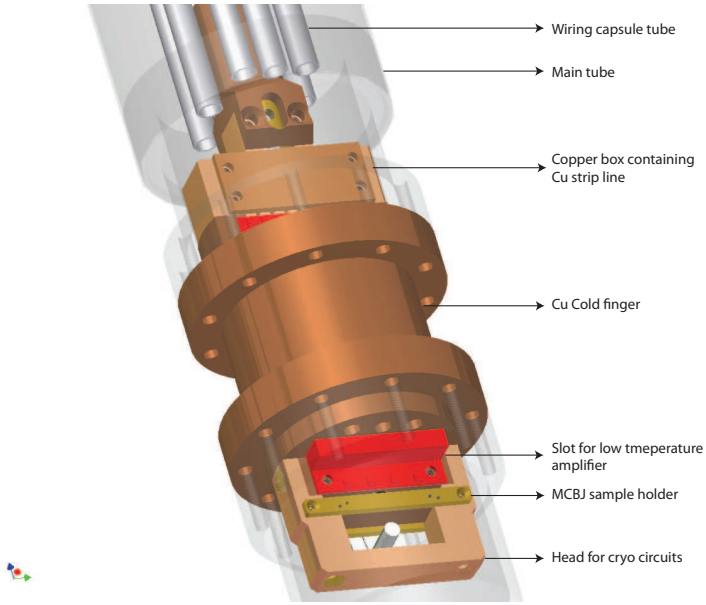

FIGURE 8.2: A 3-D view of the bottom part of the MCBJ dipstick: In the new design the dipstick has a heavy Cu block serving as a block for thermalization of the cryo-electronics. Vacuum sealing is done with Indium. The copper block connects the main tube to the sample space and the cap, and is in direct contact with the helium bath. When opening the cap the only exposed area is the input of the low temperature amplifiers and the sample. All the rest of the wiring is fixed within the copper box coupled to the top of the Cu amplifier housing.

Wiring of the dipstick

In the new design the wires running down the central tube are held by capsules, which are formed by semi-cylindrical tubes (a tube cut in half along its length). These can be inserted into the fine hollow tubes, that are coupled to the main tube of the dipstick using silver welding for good thermal and mechanical anchoring. The wires are glued onto the inside of these semi-cylindrical tubes by GE varnish with copper wool added. This has the advantage that it helps anchoring the wires thermally and mechanically to the inner wall of the rod efficiently, while the wires can be easily removed from the wiring capsule for maintainance and modifications. The wiring of the dipstick at the top and bottom of dipstick can be done independently from each other. The wiring module at the dipstick head is removable and hence is accessible for soldering.

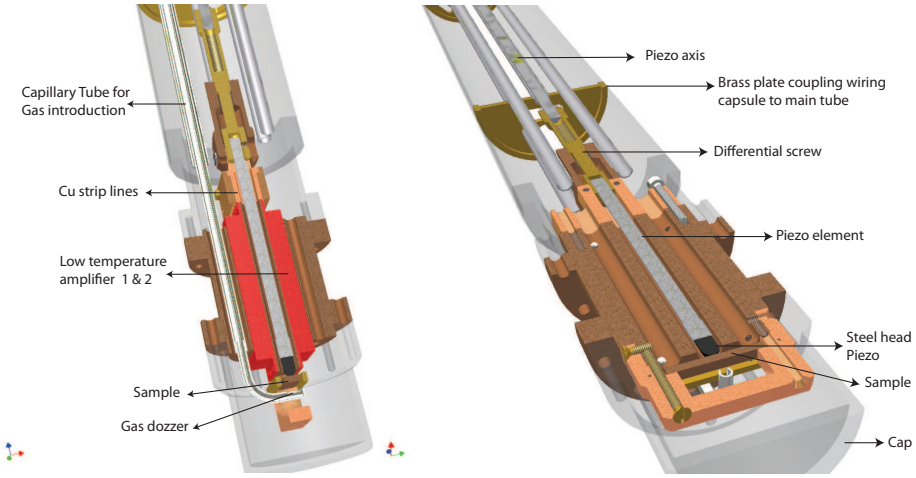

FIGURE 8.3: Cross section view of the dipstick showing the details of its cryogenic part. The large copper mass serves for thermalization and housing of the cryogenic amplifiers. The cryogenic amplifiers shown schematically in red are fixed with screws in the slots in the Cu housing. Copper wool is added between the gold plated low temperature amplifier base and the copper bock for better thermalization. The capillary tube for admitting of gases is isolated from the Cu block using a Teflon ring. The capillary tube has an extension at the cryo end with a gas dozer nozzle facing the sample. The sample sits in the slot at the end of the piezo element. Only the head of the piezo element sticks out of the central tube in the cold Cu block. All removable parts at the cryogenic vacuum end are held by brass screws. The cryogenic cap is tightened on the cryogenic Cu block using stainless steel screws and an indium seal.

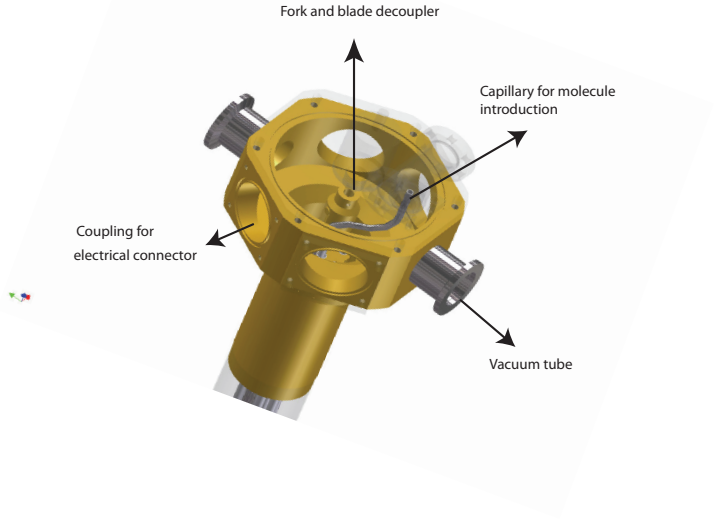

FIGURE 8.4: 3D view of the head of the dipstick. In the new design a fork-blade coupling between the external rotation drive and the screw axis is put at the top of the screw axis. Two vacuum feed throughs are welded on the head of the dipstick, while electrical feed throughs are O-ring sealed. The second stage RT amplifiers are placed inside the head of the dipstick (not shown here).

Efficient thermalization

We have taken care of proper thermalization of all wires coming from the RT head to the cryo head in two stages. All the wires coming from the RT head are manganin (Cu(86%) Mn(12%) Ni(2%)) wires, which provide a good compromise between a high electrical conductance and a low thermal conductance. These manganin wires are thermally coupled to the inner wall of the dipstick through the fixation described above, where they are cooled against the He liquid and gas temperatures inside the cryogenic vessel. All wires are soldered onto electrically isolated Cu strips on the cold finger where they are cooled efficiently by the liquid He bath. This reduces the heating of the sample and amplifier from RT phonons and also reduces the heat load on He bath, giving a longer measurement time. All the measurement wires coupling the respective strip lines to the amplifier or to the MCBJ sample are Cu wires. The screw rod is coupled to the copper block for thermalization such that it should not heat the sample during making and breaking of the contact. We have placed the copper block directly in contact with the He bath, which provides efficient thermalization of the sample and the amplifiers and gives a faster cooling time of about 2hrs to reach the base temperature of 4.2K. This is quite an improvement over the earlier designs, which give cooling times of about 6hrs to a base temperature of 5.7K.

Mechanical stability

We paid special attention to attain better mechanical stability, since the process of conductance and noise spectroscopy usually takes more than an hour and in future measurement runs stretching over more than 2hours of measurement time on a single contact setting are anticipated. Instabilities in the atomic contacts can be grouped into two classes, one inherent to the properties of the sample, *i.e.* due to the microscopic structure and atomic arrangement very close to the atomic contact, and the other due to electro-mechanical instabilities *i.e.* due to the coupling of external electro-mechanical disturbances to the atomic contact. Instabilities inherent to the sample can often be improved by annealing the sample in the cryogenic vacuum at high currents. External mechanical instabilities can be due to electrical noise on the piezo voltage, and vibrations coupling mechanically or acoustically into the setup and to the sample. Electrical noise in the piezo driver is efficiently reduced using a 3^{rd} order passive low pass filter with a cutoff frequency of 10Hz. The piezo wires are separated from the sensitive measurement wires by mounting them in separate wire tubes. At the cryo head the piezo wires are coupled to separate strip lines shielded from the measurement wires though grounded strip lines. The whole construction is inside the copper block which provides further electrical shielding. The piezo element itself is inside this copper shielding and at the sample side only the hemispherical steel head sticks out, which couples

the piezo element mechanically to the sample. This design helps in reducing the fluctuations in the high-voltage piezo drive coupling to the signal wires.

For mechanical stabilization we have decoupled the screw axis to the piezo element using a fork blade configuration, which is positioned at the top of the insert in our design. During the measurement the sample is suspended in a cryogenic vacuum. Further reduction of mechanical and acoustic disturbance is achieved in the usual way by placing the experiment inside an acoustically shielded box suspended on pneumatic vibration dampers. For sensitive measurements the turbo pump can be decoupled from the dipstick.

Efficient pumping

The main tube of the dipstick has a lot of empty space which we have tried to maximally use for pumping. We have further reduced the size of the cryogenic sample space to reduce the effective volume needed to be pumped. A container with active coal is mounted in the cryo cap for added cryogenic pumping. The reduction of the sample space helps in reducing the cool down time and increasing the measurement time.

Electromagnetic shielding

Electromagnetic shielding has been improved by using grounded strip lines as shields around the exposed naked wires. At the cryo head the cold strip lines are shielded by the copper box. The high voltage wires were kept far from the sensitive signal wires. A central star grounding scheme for all signal circuits was was used with the star point at the cryo head, in order to minimize ground loops.

8.2.2 CHARACTERIZATION OF THE DIPSTICK

The measurement properties of the new dipstick were characterized by measuring Au atomic contacts. A simplified schematic of the measurement circuit (figure (3.5)) is shown in figure (8.5). A Au atomic contact is formed by stretching a Au contact starting from a bulk contact size. The dc conductance characterization of the Au atomic contact is shown by the conductance histogram in figure (8.6). The conductance histogram shows a clear peak at $0.98G_0$, and the usual structure expected for Au. The typical traces in the inset show the formation of atomic chains. The length histogram recorded on the same contact shows the usual multiple peaks. The first inter peak distance gives the reduction factor of 0.08V/Å. The stability of the contact depends on the local atomic configuration but it is also affected by external disturbances. The fluctuations in the conductance of the Au atomic contact measured in the new dipstick are found to remain within the measurement accuracy of 1% in conductance for > 2hrs of measurement time. The average drift of the contact is less than 0.01% over the period of 2.5hrs, as shown in figure (8.7).

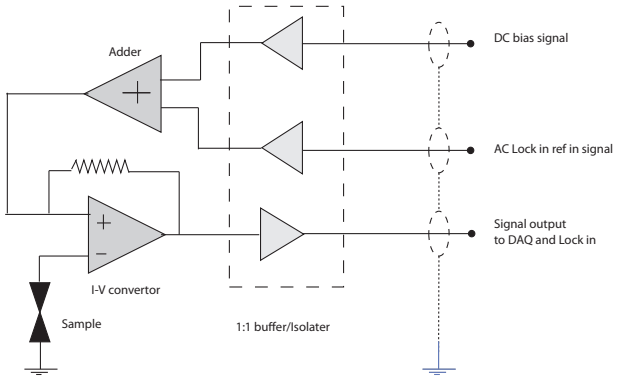

FIGURE 8.5: Circuit for conductance measurements: This is a simplified version of the circuit diagram shown in figure (3.5). The ac measurement is done using a lockin technique. The grounding of the dipstick is isolated from the ground of measurement equipment using 1 : 1 buffer amplifiers.

8.3 TWO CHANNEL SPECTRUM ANALYZER

THE high-bias noise measurements on molecular systems require extending the noise measurements into the MHz regime. We have decided to use a cross spectrum noise measurement technique, which then requires fast data acquisition and manipulation. We have adopted a National Instruments PXI-5641R data acquisition unit for the digitization of the signals. The 5641-R gives 14 bit analog to digital conversion, for single-ended AC coupled dual channels, with an analog bandwidth of 50kHz-80MHz [9]. The average input noise is $16\text{nV}/\sqrt{\text{Hz}}$ with -60dB channel-to-channel crosstalk up to 80MHz. The maximum input signal is 24dBm peak without damaging the card. A low pass filter at the input limits the band width at the lower end. In our case we have operated the unit at 10MHz band width to reduce aliasing in comparison with the 20MHz bandwidth setting. Data handling speed is accelerated by using a Virtex 5 FPGA (Field Programmable Gate Array, 94208 logic cells, 640 multipliers and 8784 block RAM) on the PXI express backplane. Due to the 32-bit PXI express bus with DMA capability data communication from the FPGA to the host computer and to FPGA from the host computer within the PXI backplane can be done above 100MB/s and 50MB/s, respectively. The combination of the PXI express bus and FPGA allows the implementation of a real time cross spectrum analyzer.

8.3.1 DATA PROCESSING

The realization of a two channel cross spectrum analyzer based on the PXI-5641R system is shown schematically in figure (8.8). The band limited noise signal is fed

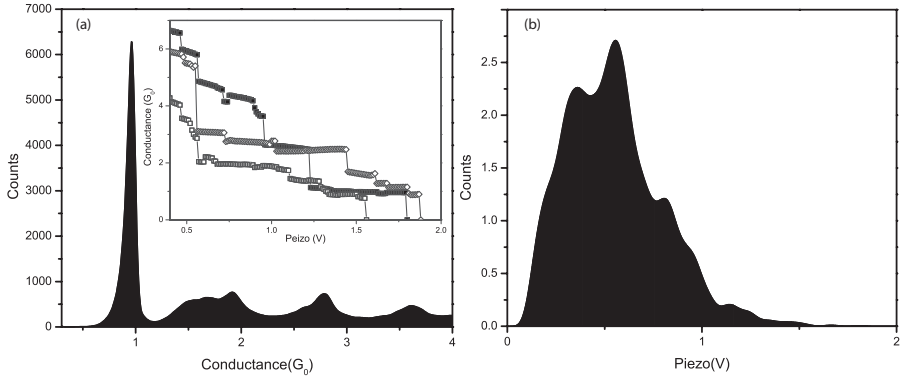

FIGURE 8.6: DC conductance characterization of the Au atomic contact in the new dipstick: A conductance histogram is recorded for Au atomic contacts. The conductance histogram shows the usual peak at $0.98G_0$. The inset shows typical traces recorded. (b) Length histogram recorded for Au atomic contacts, which also shows the usual structure with multiple peaks. The calibration factor for the new low-voltage piezo element used in this dipstick is found to be 0.08V/Å

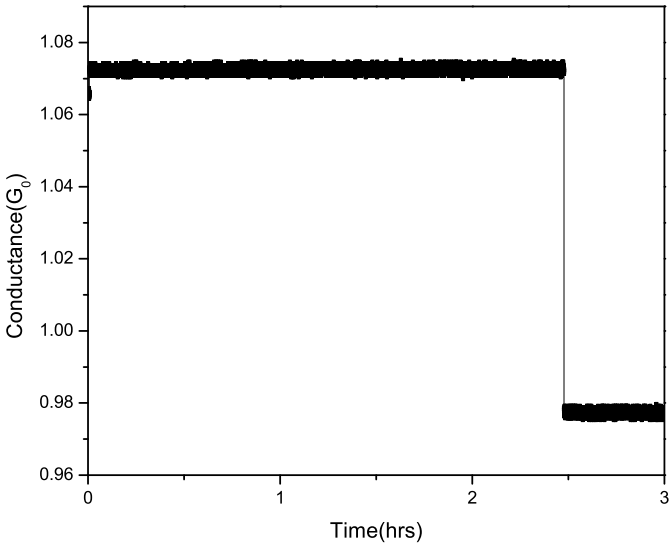

FIGURE 8.7: Stability test of a Au atomic contact in the new dipstick: An atomic contact of $1.07G_0$ is formed and the conductance is measured as a function of time until the contact is breaks. The average drift of the contact is less than 0.01% over the period of 2.5hrs.

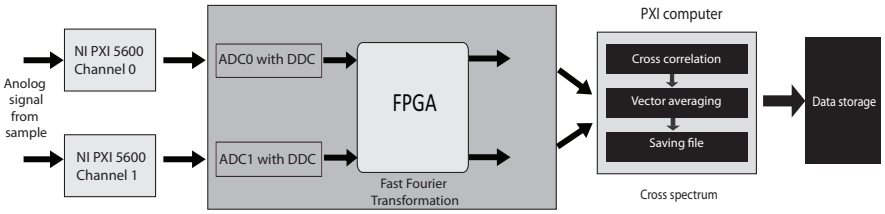

FIGURE 8.8: Data processing flow chart for the real time spectrum analyzer: The analog signals are fed into the ADC (analog-to digital conversion) channels of the 5641-R unit for digitization. The built-in FPGA unit processes a fast-Fourier transform (FFT) of the digitalized signals and the data is further processed for lower order computation (cross spectrum and vector averaging) in the host computer. The final computed data is saved on a network drive.

into the input of the data acquisition card for digitization. The sampling rate and digital down conversion (DDC) give a resolution width of ~ 12.2kHz. The outputs of both ADC/DDC channels are fed to the FPGA simultaneously. For each acquisition time series, the FPGA takes blocks of N×1024 data points and performs a complex FFT on them[1]. Here N specifies the number of averages and 1024 is number of FFT points. The outputs of the FFT are transmitted to the host computer using direct memory access (DMA). The host computer performs the lower order computations which involves cross spectrum calculations and the running vector averaging, and it takes care of saving the data on the network drive.

8.3.2 CHARACTERIZATION OF THE TWO CHANNEL SPECTRUM ANALYZER

The operation and linearity of the spectrum analyzer was verified using a band limited (20MHz) Agilent signal source (33250A). The white noise generated by the signal source was increased in steps of $1mV_{rms}$ and was fed into the two input channels of the PXI-based cross spectrum analyzer. The cross spectrum of the signal with averaging over 4000 samples was calculated using the FPGA based FFT spectrum analyzer and host computer. The raw spectra are normalized by the 1mV spectrum in order to correct for the transfer function of the measurement circuit. The normalized spectra in the window of 2MHz - 6MHz are shown in figure (8.9a). The mean values calculated from the normalized spectra are plotted *w.r.t.* input noise values in figure (8.9b). The linear response of the PXI system is confirmed by the linear fit to the experimental data points.

[1]The FPGA program was designed by Kartsen van Zwol, NI engineer using Labview FPGA and Asynchronous wire programming

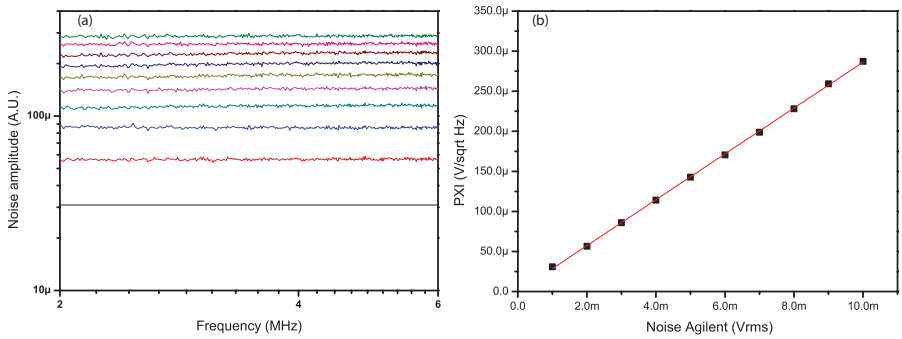

FIGURE 8.9: Test of the PXI-based cross spectrum analyzer: (a) Raw FFT spectra in the window of 2MHz-6MHz, normalized by the spectrum taken at $1mV_{rms}$ input signal. The black line shows the noise level at $1mV_{rms}$ input, used for the normalization. (b) The mean values of the normalized spectra in the window of 2MHz-6MHz are plotted *w.r.t.* to corresponding input noise values from the signal source. The straight line is a linear fit to the experimental data points.

8.4 THE CRYOGENIC AMPLIFIERS

THE cryogenic amplifiers are designed in close collaboration with Stahl Electronics. The design constraints for the amplifiers were not only given by the desired input current and voltage noise levels, but also by requirements for the effective thermalization of the all active and passive elements on the printed circuit board, and by size limitations. The main design constraints are: (1) Low current and voltage noise. (2) Low thermal load. (3) The amplifiers should fit inside a dipstick with outer diameter 50mm. (4) Long stable operation. (5) The amplifiers should operate up into the low-MHz regime.

8.4.1 AMPLIFIER DESIGN

The cryogenic amplifiers were designed inspired by the low noise amplifiers described by Adrian Tae-Jin Lee [10]. The amplifier has two stages. The first stage is a dual channel low noise cryogenic amplifier with operational frequency window of 300kHz - 30MHz. The output of this stage, with an impedance of 75Ω is coupled to the input of the second stage low noise dual channel amplifier at RT, with operational frequency window of 20kHz - 100MHz. The advantage of this design is the low heat load on He bath and the smaller size of the cryogenic amplifier. For the cryogenic stage we have used high electron mobility transistors (HEMT), and Si FET's for the RT stage amplifier [11, 12]. In our design the heat load on the He bath is 1.2mW. The main disadvantage of this design is that the noise of the RT amplifier dominates the noise performance [13]. This is also a reason why we are using the cross spectrum measurement technique.

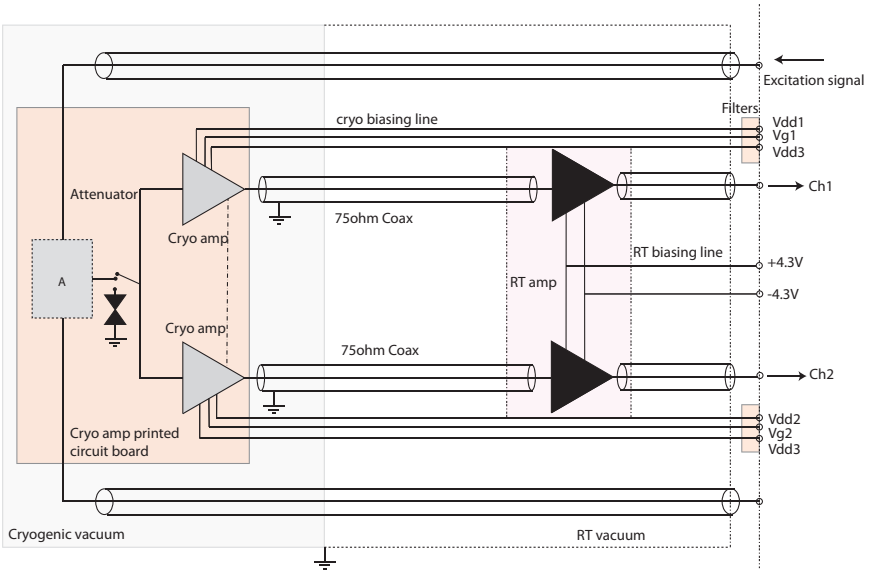

FIGURE 8.10: Schematic of the low noise amplifier: A two stage dual channel single ended low noise amplifier was realized. The power biasing lines are fitted with optional low pass filters. The excitation line is incorporated in the design for gain calibration purposes. The attenuator close to the input of the amplifier is also optional and in the current version it is omitted. The Cu cold block of the dipstick is made the ground point for the cryo circuit. The cascode stage of each channel has independent biasing parameters while the source follower of both channels have a common biasing line. This gives five independent bias voltage settings.

The design of the biasing circuitry and the conceptual design of the cryogenic amplifier is shown in figure (8.10). The cryo end of the amplifier acts as impedance transformer with a gain of 6.3X. All transistors used in the cryogenic stage are HEMT transistors because of their low noise and lower power dissipation performance at cryogenic temperatures. For Si based transistors the mobile charges would freeze out at low temperatures and would require a sophisticated heating of the amplifier and its isolation from the 4K bath. GaAs based transistors are prone to large low frequency 1/f noise. The cryogenic amplifier is based on cascode biasing to the source follower. The cascode stage eliminates the Miller effect, which is the drain to gate capacitive feedback. The Miller effect also decreases the stability of the circuit at higher frequencies, where effective feedback is positive due to the large phase shift ($> 180^\circ$) between the input and the feedback signal. This feedback limits the upper cutoff frequency in the source follower circuit. The source follower is a low input impedance transimpedance amplifier. It converts the cur-

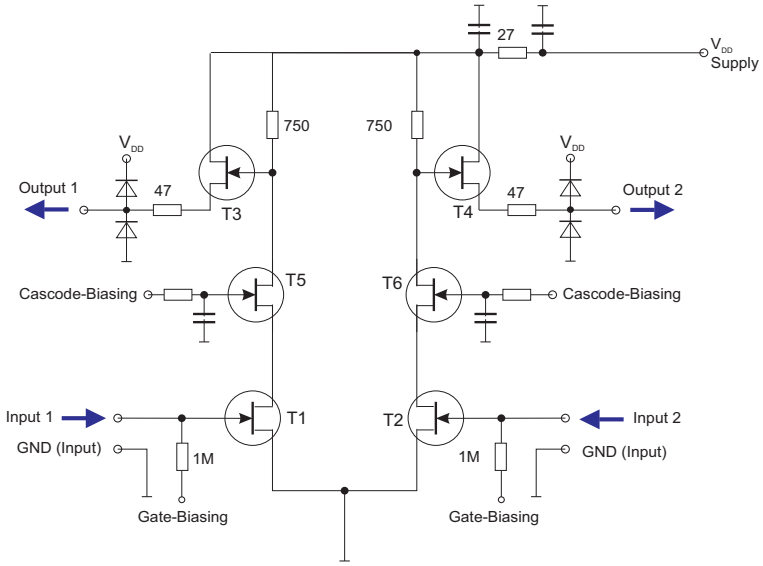

FIGURE 8.11: Schematic of the cryogenic low noise amplifier stage: The gate of the source follower is biased using a cascode stage transistor. This design gives a broadband frequency response in the low-MHz regime. The cascode biasing of the source follower is used to minimized the Miller effect. Both channels are mounted on the same printed circuit board. Apart from the source follower biasing for both channels the cascode biasing can be tunned independently.

rent fluctuations to voltage fluctuations through the source-drain resistance. The other advantage of the source follower is that the output impedance of this stage matches the cable impedance hence improves the high frequency performance.

A circuit diagram of the RT amplifier is shown in figure (8.12). The gain of the cryogenic amplifier should be high enough such that its output signal dominates the input noise of the RT amplifier (see also section 2.1.1). The effective gain of the cryogenic amplifier is approximately 5X. The input of RT amplifier is coupled to the output of the cryogenic amplifier through a transformer. The purpose of the transformer is to have better impedance matching and it reduces high frequency oscillations. The RT amplifier has a gain of 10X. The input impedance is 75Ω matching the output impedance of the cryogenic amplifier. The RT amplifier has a fixed biasing point using two voltage supplies at +4.3V and −4.3V. The RT amplifier is mounted inside the brass head at the top of the dipstick. Proper thermal anchoring is provided for stable operation of the device. The output line is protected from spurious static discharges by a buffer amplifier and diode. The output of the RT amplifier is coupled to next stage amplifier through 50Ω coax cables.

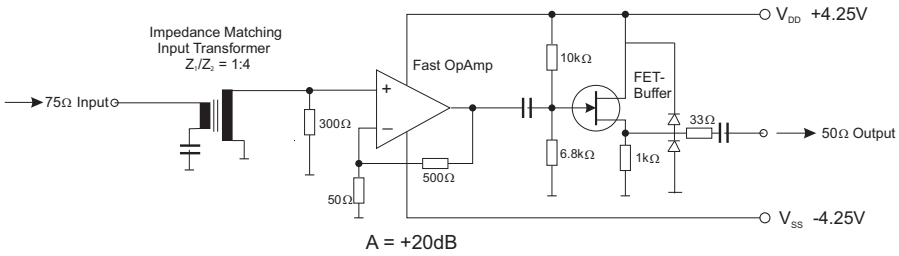

FIGURE 8.12: Circuit diagram of the RT low noise amplifier: Here only a single channel of the amplifier is shown. The output of the cryogenic amplifier is coupled to the RT stage of the low noise amplifier through an impedance transformer. The output of the high frequency Opamp is protected using a buffer amplifier and diode. The gain of the Opamp is approx. 20dB.

8.4.2 CHARACTERIZATION OF THE AMPLIFIER

The cryo and RT amplifiers were characterized independently. The voltage noise of the RT amplifier is shown in figure (8.13a). The input noise of the RT amplifier in the frequency window of 300kHz - 10MHz is approximately 2.5nV/$\sqrt{\text{Hz}}$. The noise performance degrades somewhat at the higher frequency end. At lower frequencies $1/f$ noise takes over, superimposed with several resonances. This $1/f$ noise is common for Si based transistors. Here, input current noise is not significant due to the small output impedance of the cryogenic stage amplifier. A gain-bandwidth measurement for the RT amplifier is shown in figure (8.13b). The gain for the two channels closely matches for the same ±4.3V biasing. The effective 3dB bandwidth of the RT amplifier is 400kHz - 60MHz. The spectrum is relatively flat between 300kHz - 10MHz. The total amplification in this window is 22.5dB.

The noise characterization of the cryo amplifier stage is shown in figure (8.14a). The biasing parameters used for this measurement are $V_{dd1} = 2.00$V, $V_{dd2} = 2.00$V, $V_{dd3} = 2.55$V, $V_{g1} = -0.40$V, $V_{g2} = -0.43$V. The voltage noise is determined using a shorted input of the amplifier, while the current noise is measured with a 11.5pF capacitor connected over the input and subtracting the voltage noise from the total noise. The voltage and current noise of the amplifier are found to be 0.9nV/$\sqrt{\text{Hz}}$ and 50fA/$\sqrt{\text{Hz}}$, respectively. The gain-bandwidth characteristics is shown in figure (8.14b). The characteristics of the two channels matches within 3dB between 1MHz and 28MHz. The average gain of the amplifiers in this window is 16dB. The antiresonance at 29MHz is due to an instability of the source follower due to high frequency feedback.

In our low noise amplifier design both channels for the cryogenic amplifier and RT amplifier are on same board and hence could couple capacitively, which could give rise to cross talk. A measurement of the cross talk for the RT amplifier is given

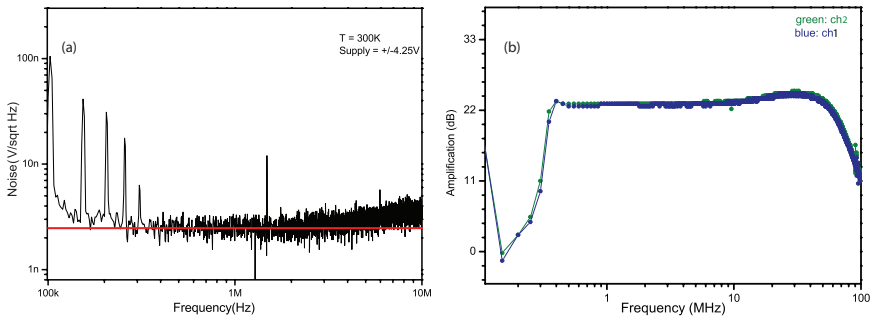

FIGURE 8.13: Gain and noise characterization of the low-noise amplifiers: (a) Noise characteristics of the RT amplifier stage. The voltage noise in the relevant frequency window is approx. 2.5nV/$\sqrt{\text{Hz}}$. (b) The effective gain of the RT amplifier is 22.5dB, or 13.1X, closely matched for the two channels, shown separately in blue and green.

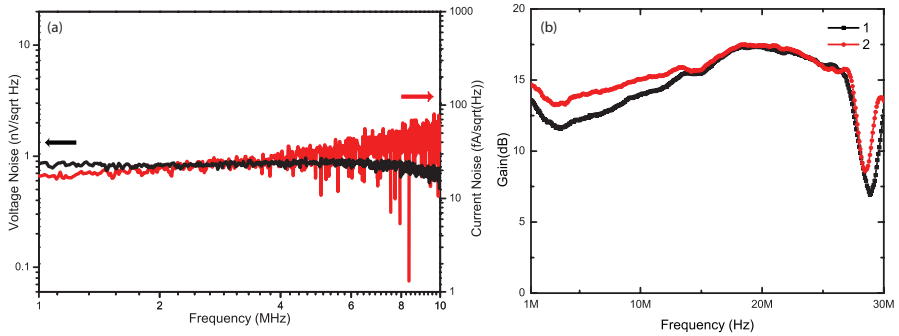

FIGURE 8.14: Gain and noise characterization of the low-noise amplifiers: (a) Voltage noise (black) and current noise (red) for the low noise cryogenic amplifier stage. The voltage noise and current noise are found to be approximately 0.9nV/$\sqrt{\text{Hz}}$ and 50fA$\sqrt{\text{Hz}}$. (b) The gain-bandwidth plot shows an effective gain of 16dB, or 6.3X.

8

in figure (8.15). The cross talk between the two channels for the cryo amplifier is expected to be similar. The data around 1MHz show effectively 38dB, or 1.2%, of signals parasitically coupled to each other. This could be further improved by using two separate printed circuit boards for the two channels.

The effective noise contributed by the low noise amplifier in each channel is given by

$$V_n^2 = v_n^2 + i_n^2|Z_{in}|^2 + c_n^2|iZ_{in}|^2 \tag{8.1}$$

Here v_n and i_n are the voltage and current noise at the input of the amplifier, respectively, while the c_n is the correlated noise, which could be due to cross talk or

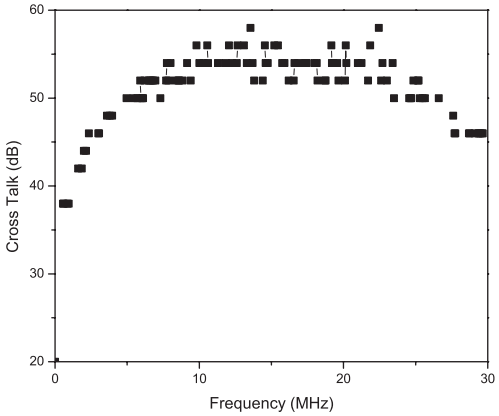

FIGURE 8.15: Cross talk for the RT stage of the low noise amplifier. The discreteness in data is due to the digital resolution setting of the spectrum analyzer.

residual correlations. The first term can be removed by using the cross spectrum measurement, while the last two terms adds up in the noise spectra, and this limits our noise measurement resolution.

8.5 FURTHER IMPROVEMENT

The current setup was designed around the implemented cryogenic amplifiers in the noise measurement circuit. Although the system is quite modular, it has its own complexity too. A few modifications could be implemented into the design of the cryo part of the dipstick. A cooling pad could be mounted on the sample side of the Cu cold block. This would give improved ease of soldering and re-soldering of the wires without dismantling the cold block from the dipstick. Although the dipstick has a quite good mechanical stability, this could be improved further by having the fork-blade decoupler at the cryo side rather than at the RT head of the dipstick. The low noise amplifier as it is now has its input noise dominated by the RT stage amplifier, which could be compensated for by increasing the transimpedance of the cryo side of the amplifier. The matching of the two channels of the cryo amplifier could be further improved. The PXI cross spectrum analyzer is working in principle, but the speed of data processing can be improved by using the FPGA for the lower order computation also.

The conceptual design of the high frequency noise measurement setup in the low MHz regime has been realized and characterized, but it needs a few further steps to be completed. Noise spectroscopy for actual atomic contacts needs to

be tested. The combination of the noise measurement setup with the present conductance measurement circuit will reduce the intrinsic high frequency cutoff back to a few hundred kHz. To prevent this requires decoupling the conductance measurement circuit from the noise measurement circuit. We have tried to use a cryogenic electro-mechanical switch for this purpose, however we found that this switch introduces electrical and mechanical pulses that lead to breaking of the atomic contact during the switching. We presently aim for adding a cryogenic amplifier for the conductance measurement circuit which will decouple the wire capacitances from the sample. This will give the capability of doing the both dc and ac conductance measurements and noise measurement on the same atomic point contact.

REFERENCES

[1] M. Kumar, R. Avriller, A. L. Yeyati, and J. M. van Ruitenbeek, *Detection of vibration-mode scattering in electronic shot noise.*, Physical review letters **108**, 146602 (2012).

[2] D. Djukic, K. S. Thygesen, C. Untiedt, R. H. M. Smit, K. W. Jacobsen, and J. M. van Ruitenbeek, *Stretching dependence of the vibration modes of a single-molecule* $Pt-H_2-Pt$ *bridge*, Phys. Rev. B **71**, 161402 (2005).

[3] W. Thijssen, D. Marjenburgh, R. Bremmer, and J. van Ruitenbeek, *Oxygen-Enhanced Atomic Chain Formation*, Physical Review Letters **96**, 0268061 (2006).

[4] Y. P. Li, D. C. Tsui, J. J. Heremans, J. A. Simmons, and G. W. Weimann, *Low frequency noise in transport through quantum point contacts*, Applied Physics Letters **57**, 774 (1990).

[5] F. Liefrink, J. I. Dijkhuis, and H. van Houten, *Low-frequency noise in quantum point contacts*, Semiconductor Science and Technology **9**, 2178 (1994).

[6] T. Delattre, C. Feuillet-Palma, L. G. Herrmann, P. Morfin, J.-M. Berroir, G. Fève, B. Plaçais, D. C. Glattli, M.-S. Choi, C. Mora, et al., *Noisy Kondo impurities*, Nature Physics **5**, 208 (2009).

[7] H. Birk, M. J. de Jong, and C. Schonenberger, *Shot-Noise Suppression in the Single-Electron Tunneling Regime*, Phys. Rev. Lett. **75**, 1610 (1995).

[8] I. T. Vink, T. Nooitgedagt, R. N. Schouten, L. M. K. Vandersypen, and W. Wegscheider, *Cryogenic amplifier for fast real-time detection of single-electron tunneling*, Applied Physics Letters **91**, 123512 (pages 3) (2007).

[9] N. Instrument, Tech. Rep., National Instrument (2009), URL `http://www.ni.com/pdf/manuals/375120b.pdf`.

[10] A. T. Lee, *Broadband cryogenic preamplifiers incorporating GaAs MESFETs for use with low temperature particle detectors*, Review of Scientific Instruments **60**, 3315 (1989).

[11] J. Bautista, Tech. Rep., Radio frequency and Microwave subsystems, NASA (1993).

[12] Z. Svindrych, Z. Janua, F. Soukup, and R. Tichy, *Operational amplifiers operating in temperature range from 300 to 4.2K*, Cryogenics **48**, 160 (2008).

[13] L. K. J. Vandamme, in *Advanced Experimental Methods for Noise Research in Nanoscale Electronic Devices, Proceedings of the NATO Advanced Research Workshop, Nato Science Series II* (2003), vol. 151, pp. 1–370, URL http://rd.springer.com/book/10.1007/1-4020-2170-4/page/1.